

THE STATE OF THE CIRCUMSTELLAR MEDIUM SURROUNDING GAMMA-RAY BURST SOURCES AND ITS EFFECT ON THE AFTERGLOW APPEARANCE

ENRICO RAMIREZ-RUIZ^{1,2}, GUILLERMO GARCÍA-SEGURA³, JAY D. SALMONSON⁴, AND BRENDA
 PÉREZ-RENDÓN^{3,5}
Draft version March 17, 2019

ABSTRACT

We present a numerical investigation of the contribution of the presupernova ejecta of Wolf-Rayet stars to the environment surrounding gamma-ray bursts (GRBs), and describe how this external matter can affect the observable afterglow characteristics. An implicit hydrodynamic calculation for massive stellar evolution is used here to provide the inner boundary conditions for an explicit hydrodynamical code to model the circumstellar gas dynamics. The resulting properties of the circumstellar medium are then used to calculate the deceleration of a relativistic, gas-dynamic jet and the corresponding afterglow light curve produced as the shock wave propagates through the shocked-wind medium. We find that variations in the stellar wind drive instabilities that may produce radial filaments in the shocked-wind region. These comet-like tails of clumps could give rise to strong temporal variations in the early afterglow lightcurve. Afterglows may be expected to differ widely among themselves, depending on the angular anisotropy of the jet and the properties of the stellar progenitor; a wide diversity of behaviors may be the rule, rather than the exception.

Subject headings: gamma-rays: bursts — ISM: jets and outflows — radiation mechanisms: non thermal — polarization — relativity — shock waves

1. INTRODUCTION

Over the past six years evidence has mounted that long-duration (≥ 2 s) gamma-ray bursts (GRBs) signal the collapse of massive stars in our Universe. This evidence was originally based on the probable association of the unusual GRB 980425 with a type Ib/c supernova (SN; Galama et al. 1998) but now includes the association of GRBs with regions of massive star formation in distant galaxies (Paczynski 1998; Wijers et al. 1998; Fruchter et al. 1999; Djorgovski et al. 2001; Trentham et al. 2002), the appearance of supernova-like *bumps* in the optical afterglow light curves of several bursts (Bloom et al. 1999; Zeh, Klose & Hartmann 2004 and references therein), lines of freshly synthesized elements in the spectra of a few X-ray afterglows (Piro et al. 2000; Reeves et al. 2002), and the first convincing spectroscopic evidence that a very energetic supernova (a hypernova) was temporally and spatially coincident with a GRB (Hjorth et al. 2003; Stanek et al. 2003). These observations support the idea that long-duration GRBs are associated with the deaths of massive stars, presumably arising from core collapse (Woosley 1993, Zhang et al. 2003).

An implication of a massive star progenitor is that the circumburst environment is determined by the mass-loss wind from the star. Much of our effort in this paper will therefore be dedicated to determining the state of the circumburst material in various types of progenitor scenarios, and describing how this external matter can affect GRB jets propagating through it. Because massive stars are expected to have their close-in surroundings modified by the progenitor winds, we consider both free winds and shocked winds as possible surrounding media for the afterglow stage. Detailed hydrodynamic simulations of this interaction are presented in §4. An understanding of the evolution of a gas-dynamic jet can come only through a knowledge of the properties of the medium which it propagates. Calculations of the evolution of a relativistic, gas-dynamic jet and expected emission properties are discussed in §5. For completeness, the interactions with either a free wind or a constant density medium, as well as the termination shock wave which marks the transition between these two media, are discussed in §2 and §3. We then in §6 discuss the possible variety of afterglow variability that is expected from GRB jets expanding in a medium that may be inhomogeneous because of clumping in the Wolf-Rayet (WR) star wind. Discussion and conclusions are presented in §7.

2. THE CIRCUMBURST MEDIUM

If the progenitors are massive stars then there is an analogy to the explosions of core collapse supernovae, for which there is abundant evidence that they interact with the winds from the progenitor stars. In most supernova cases, the radial range that is observed is only out to a few pc, such that the mass loss characteristics have not changed significantly during the time that mass is supplied to the wind (Chevalier & Li 2000). The density in the wind depends on the type of progenitor. Red supergiant stars, which are thought to be the progenitors of Type II supernovae, have slow dense winds. Wolf-Rayet stars, which are believed to be the progenitors of Type Ib/c supernovae and possibly of GRBs (e.g. MacFadyen & Woosley 1999; Izzard et al. 2004), have faster, lower-density winds.

The winds from typical red supergiants are slow-moving and dense, with velocities $v_w \approx 10\text{--}20\text{ km s}^{-1}$ and mass loss rates between 10^{-6} and $10^{-4}\text{ M}_{\odot}\text{ yr}^{-1}$. As a *representative* red supergiant wind consider the case of SN 1993J. In a steady, spherically symmetric

¹ Institute for Advanced Study, Einstein Drive, Princeton, NJ 08540; enrico@ias.edu

² Chandra Fellow

³ Instituto de Astronomía-UNAM, Apartado Postal 877, Ensenada, 22800 Baja California, Mexico; ggs@astrosen.unam.mx.

⁴ Lawrence Livermore National Laboratory, Livermore, CA 94551; salmonson@llnl.gov

⁵ Universidad de Sonora, Hermosillo, Sonora, Mexico

wind the electron density drops as $n_w(r) = \dot{M}/(4\pi v_w r^2 \mu_e m_p)$, where μ_e is the molecular weight per electron. Deviations from an r^{-2} density gradient towards a flatter slope, $n_w \propto r^{-1.5}$, have been inferred in the circumstellar medium of this supernova by Fransson et al. (1996), and are possibly caused by a variation of the mass-loss rate from the progenitor or by a non-spherical geometry. Following Fransson et al. (1996) one can write

$$n_w(r) \approx 10^8 \text{ cm}^{-3} r_{15}^{-3/2} \dot{M}_{-4.4} v_{w,1}^{-1} \quad (1)$$

up to $r = 2 \times 10^{16} \text{ cm}$, while at larger radii the observations appear to be consistent with a r^{-2} law. Here $v_w = 10 v_{w,1} \text{ km s}^{-1}$, $r = 10^{15} r_{15} \text{ cm}$, and $\dot{M} = 4 \times 10^{-5} \dot{M}_{-4.4} M_\odot \text{ yr}^{-1}$. The winds from WRs, on the other hand, are characterized by mass-loss rates $\dot{M} \approx 10^{-5} - 10^{-4} M_\odot \text{ yr}^{-1}$ and velocities $v_w \approx 1000 - 2500 \text{ km s}^{-1}$ (e.g. Chiosi & Maeder 1986). In a steady, spherically symmetric wind, the electron density is

$$n_w(r) \approx 3 \times 10^6 \text{ cm}^{-3} r_{15}^{-2} \dot{M}_{-4} v_{w,3}^{-1} \mu_e^{-1}, \quad (2)$$

where $\mu_e \sim 2$ in a helium gas.

For this discussion we shall assume the blast wave is adiabatic, i.e. its energy is constant with time, and effectively spherical. This means the E here is the isotropic equivalent energy as, for example, derived from the gamma-ray output. Deceleration due to the stellar wind starts in earnest when about half the initial energy is transferred to the shocked matter, i.e. when it has swept up γ^{-1} times its own rest mass. The typical mass where this happens is

$$M_{\text{dec}} = \frac{E}{\gamma^2 c^2} \approx 5 \times 10^{-6} E_{53} \gamma_{0.2}^{-2} M_\odot. \quad (3)$$

The relativistic expansion is then gradually slowed down, and the blast wave evolves in a self-similar manner with a power-law lightcurve. This phase ends when so much mass shares the energy that the Lorentz factor, γ , drops to 1. Obviously, this happens when a mass E/c^2 has been swept up. This sets a non-relativistic mass scale

$$M_{\text{NR}} = \frac{E}{c^2} \approx 6 \times 10^{-2} E_{53} M_\odot. \quad (4)$$

Beyond this point, the event slowly changes into a classical Sedov-Taylor supernova remnant evolution, leading to a steeper decline in the lightcurve (Waxman et al. 1998).

In the unshocked wind, the mass within radius r is $\dot{M}r/v_w$, which combined with equation (3) gives the blast wave deceleration radius in a stellar wind:

$$r_d^w = \frac{E v_w}{\dot{M} c^2 \eta^2} \approx 2 \times 10^{15} E_{52} v_{w,3} \dot{M}_{-6}^{-1} \gamma_2^{-2} \text{ cm}, \quad (5)$$

where $E_{52} = (E/10^{52})$ ergs. By contrast, the well-known expression for the uniform-medium deceleration radius is

$$r_d = 5 \times 10^{17} (E_{52}/n_{\text{ism},0})^{1/3} \gamma_2^{-8/3} \text{ cm}, \quad (6)$$

and so a blast wave in a wind decelerates at a much smaller radius. The deceleration time is given by $t_d = r_d/(2\gamma^2 c)$ in both cases, and thus is correspondingly smaller for the wind case. However, because the Lorentz factor decreases as $M^{-1/2}$ (with M being the swept-up mass) beyond this point, the mass-starved wind blast wave decelerates much more slowly, and therefore begins to catch up. There is therefore not much difference in size between wind and uniform CM blast waves in the most commonly observed interval from 0.3 to 10 days after the burst (Fig. 1). Usually in the study of afterglows, one considers either the uniform ambient medium case or the $1/r^2$ wind case on its own⁶. However, since the wind of a star meets the interstellar medium (ISM) at some point, the density structure is more complex, and it is to this problem that we now turn our attention.

3. WIND-ISM INTERACTION

During the evolution of a wind-driven circumstellar shell the system has a four-zone structure (analogous to that of a supernova shell; Woltjer 1972). From the inside to the outside these zones are: (a) a supersonic stellar wind with density $\rho(r) = \dot{M}/4\pi r^2 v_w$; (b) a hot, almost isobaric region consisting of shocked stellar wind mixed with a small fraction of the swept-up interstellar gas; (c) a thin, dense, cold shell containing most of the swept-up interstellar gas; (d) ambient interstellar gas of number density n_{ism} (Fig. 2).

The wind initially expands unopposed into the ISM with a velocity of about $v_w \sim v_\infty$, the escape velocity at the sonic point. The free expansion phase is considered to be terminated at a time $t_{w,d}$, when the swept-up mass of the interstellar medium is comparable to the mass in the wind. The mass lost by the star is $\dot{M} t_{w,d}$ and the swept-up mass is $\frac{4\pi}{3} (v_w t_{w,d})^3 n_{\text{ism}} m_p \mu_e$. These two masses are equal when $t_{w,d} = [3\dot{M}/(4\pi v_w^3 n_{\text{ism}} m_p \mu_e)]^{1/2}$, which is about 100 years for a typical WR wind expanding into an homogeneous ISM. The free-expansion phase takes place at the early stages of the evolution of the hot star and occupies a minimal fraction of its lifetime. During this time both \dot{M} and v_w are approximately constant, and the wind bubble has reached a radius of $\sim 9 \times 10^{17} \dot{M}_{-5}^{1/2} n_{\text{ism},1}^{-1/2} v_{w,3}^{-1/2} \text{ cm}$, where \dot{M} is the mass loss rate in units of solar masses per year, and n_{ism} is the density of the surrounding medium in units of cm^{-3} .

⁶ Although the interstellar and wind models are the two main types of environments considered for afterglows, there is a different scenario involving a massive star in which the supernova explosion occurs before the GRB (Vietri & Stella 1998). The supernova would expand into the progenitor wind, creating a complex circumburst region in the inner part of the wind. Konigl & Granot (2002) have recently shown, for the case of a pulsar-wind bubble, that the shocked wind has a roughly uniform density, similar to that found in the normal interstellar medium.

When the free-expansion phase (a) has ended, the wind encounters an inward facing shock. Kinetic energy is deposited in the shocked wind region in the form of heat,

$$T_{\text{shock}} = \frac{3}{16} \frac{m_p \mu_e}{k} (\Delta v_w)^2 = 1.4 \times 10^5 \left(\frac{\Delta v_w}{100 \text{ km s}^{-1}} \right)^2 \text{ K}, \quad (7)$$

where Δv_w is the relative speed of the material approaching the shock. Thus, a jump in velocity by 800 km s^{-1} , which is still well below typical terminal wind speeds, produces a 10^7 K gas in the shocked wind region. During phase (b), the material is so hot that it causes the contact surface to expand outward more slowly than it would in a freely expanding wind. The ISM that enters the outward facing shock is heated to a temperature below 10^6 K , emission of line radiation becomes the dominant cooling process and the swept-up gas cools quickly to temperatures of about 10^4 K that can be maintained by the radiation field of the star. The duration of the adiabatic expansion phase can thus be estimated by finding the time it takes the expanding gas to cool from $T_{\text{shock}} \approx 10^7 \text{ K}$ to 10^6 K . Using equation (7), we find that a change in temperature from 10^7 K to 10^6 K corresponds to a change in jump velocity by a factor of $\sqrt{10}$. This change in jump velocity corresponds to a phase (b):(a) age ratio of about 6 (Castor et al. 1975). Thus, the age of the adiabatic phase is less than about 1000 years.

The mass of the swept-up material is much larger than that in the hot wind and, because it is cool, it lies in a compressed region. Phase (c) persists for as long as the star is able to sustain a powerful wind. The dominant energy loss of region (b) is work against the compressed region (c). The compressed region (c) expands because its gas pressure is higher than that of the surrounding ISM. Therefore, the expansion is described by the momentum equation,

$$\frac{d}{dt}[M_S(t)v(t)] = 4\pi r^2(t)P_i, \quad (8)$$

where P_i is the internal pressure of the compressed region, assuming that most of the swept-up interstellar mass remains in the thin shell. $M_S(t)$ is the mass of the shell of swept-up material, given by $M_S(t) = (4/3)\pi r^3(t)\rho_i$. P_i is determined by the gas pressure of the high temperature gas in region (b). The wind material that enters the backward-facing shock is hot, but the material that enters the forward-facing shock is cool. The cooled swept-up material is driven outward by the high gas pressure of the hot bubble. The stellar wind adds energy to region (b) at a rate

$$L(t) = \frac{1}{2} \dot{M}(t)v_w^2(t). \quad (9)$$

The internal energy in the bubble is given by the product of the energy per unit mass of the material, $(3/2)nkT/\rho_i = (3/2)P_i/\rho_i$, and the total mass of the bubble, $(4/3)\pi r^3\rho_i$. Since the total internal energy of the bubble comes from the energy of the wind, we find $\dot{P}_i = L(t)/[2\pi r^3(t)]$.

The expansion of the bubble during the adiabatic phase can be found numerically by using this expression in the momentum equation. If the wind power L is roughly constant for a period of time, t , one can write $P_i = L t / (2\pi r^3)$. The resulting solution of equation (8) gives $r(t) \propto t^{3/5}$. This shows that the shell expands more slowly than would a freely expanding wind. Since the gas in the cavity moves subsonically its pressure keeps it approximately at uniform density. The bubble could continue to expand until stalled by the pressure of the ISM (García-Segura & Franco 1996).

The radius of the wind termination shock at the inner edge of the wind bubble can be found by balancing the wind ram pressure with the post-shock cavity pressure. For a star that loses mass at a rate $10^{-6} \dot{M}_6 M_\odot \text{ yr}^{-1}$ with a wind velocity $10^3 v_{w,3} \text{ km s}^{-1}$ in interstellar gas with density $10^3 n_{\text{ism},3} \text{ cm}^{-3}$, we have a inner termination shock radius

$$r_t(t) = 0.4 \dot{M}_6^{3/10} v_{w,3}^{1/10} n_{\text{ism},3}^{-3/10} t_6^{2/5} \text{ pc}, \quad (10)$$

where $10^6 t_6$ is the lifetime of the star in Myr. The density in the uniform shocked wind region, n_{sw} , at late times is given by

$$n_{\text{sw}} \sim 3 \dot{M} \frac{t}{4\pi r_t^3 m_p} = 0.06 \dot{M}_6^{4/5} n_{\text{ism},3}^{3/5} v_{w,3}^{6/5} t_6^{-4/5} \text{ cm}^{-3}, \quad (11)$$

which shows that even if the progenitor star is embedded in a dense molecular cloud the observed blast wave can propagate in a low-density, uniform medium (Wijers 2001). The mass within the $1/r^2$ wind, M_t , is

$$M_t \sim 3 \times 10^{-4} \dot{M}_6^{13/10} v_{w,3}^{-9/10} n_{\text{ism},3}^{-3/10} t_6^{2/5} M_\odot. \quad (12)$$

Comparison with estimates given in Soderberg & Ramirez-Ruiz (2002) show that if the wind is particularly weak (i.e. $\dot{M} \leq 10^{-6} M_\odot \text{ yr}^{-1}$) or the surrounding density is high ($n_{\text{ism}} \geq 10^3 \text{ cm}^{-3}$), r_t falls within the range of the relativistic expansion. Models and observations of Galactic Wolf-Rayet stars, however, show that the swept-up shell of a red supergiant material at the outer radius is at a distance $\geq 3 \text{ pc}$ from the star (García-Segura et al. 1996a). This radius is sufficiently large that the interaction with the free $1/r^2$ wind is expected over the typical period of observation of afterglows.

Among the afterglows that can be interpreted as interaction with a undisturbed stellar wind, the highest density objects are compatible with expectations for the wind from a typical Wolf-Rayet star (Panaitescu & Kumar 2002), but the lower densities imply a wind densities that are lower by a factor of $10-10^2$. As proposed by Wijers (2001), the low-density requirement may be alleviated by appealing to a shocked wind, but the observable afterglow transitions due to the blast wave traversing the wind termination shock wave (Fig. 2) have not been seen in any afterglow.

Depending upon the wind history of a massive star during its last few centuries, however, the density structure in this inner region (i.e. relevant to the afterglow phase) could be quite complicated as the star enters advanced burning stages unlike those in any Wolf-Rayet star observed so far. The non-steady nature of the winds in massive stars therefore leaves open the possibility of interaction with denser material at early times (Chevalier et al. 2004). This encourages us to present a detailed account of the large and small scale features that may be present in the circumstellar gas distribution. These features, as we argue, can result naturally when one takes into account the complete mass-loss history of a massive star.

4. WIND-WIND INTERACTION

The detailed dynamical evolution of the circumstellar material (CSM) around massive stars is complex. Some stages of it do not involve major hydrodynamical instabilities and can thus be studied analytically by means of self-similar solutions (Weaver et al. 1977; Ostriker & McKee 1988; Chevalier & Liang 1989; García-Segura & Mac Low 1995a). However, the frequent occurrence of instabilities requires two – or three – dimensional hydrodynamic calculations in order to follow the non-linear evolution of the resulting structures (Franco et al. 1991; Blondin & Lundquist 1993; García-Segura & Mac Low 1995b).

In an effort to achieve full consistency between stellar and circumstellar evolution, we have performed several computations where the time-dependent input for the calculation of the circumstellar gas dynamics is derived from the output of a stellar evolution code developed at the University of Göttingen (Langer et al. 1988, Langer 1991). Here we carry out computational simulations with the hydrocode ZEUS-3D (version 3.4) developed by M. L. Norman and the Laboratory for Computational Astrophysics. ZEUS-3D is a finite-difference, fully explicit, Eulerian code (Clarke 1996) descended from the code described by Stone & Norman (1992). We used spherical coordinates for our simulations, with a symmetry axis at the pole, and reflecting boundary conditions at the equator and the polar axis. The reader is referred to García-Segura et al. (1996a,b) for a review of the applied computational methods and techniques.

As a first example, we follow the dynamics of the circumstellar medium around a $29 M_{\odot}$ star at the ZAMS, which evolves (at solar metallicity) through a long-lived red supergiant (RSG) stage with prominent consequences for the evolution of the circumstellar matter. The $29 M_{\odot}$ stellar model has steady winds during the main-sequence (MS) and RSG stages. For that reason, the CSM evolution during these stages is computed in one dimension for a homogeneous ISM. For the calculation of the post-RSG evolution the variables such as the temperatures and density are extrapolated onto a two dimensional grid. Note, however, that the calculations start before the RSG phase has ended in order to be sure that the RSG shell is dynamically stable. The total amount of mass lost by the RSG in the wind is $M_{\text{rsg}} = 10 M_{\odot}$, with a mass loss rate $\dot{M}_{\text{rsg}} = 6 \times 10^{-5} M_{\odot} \text{yr}^{-1}$ and wind velocity $v_{\text{rsg}} \sim 15 \text{ km s}^{-1}$.

When the fast WR wind $v_w \sim 3500 \text{ km s}^{-1}$ starts blowing, it sweeps up the RSG wind material into a shell, which we will refer to as the *WR shell*. The properties of this shell turn out to be very sensitive to the characteristics of the RSG wind. Since the density of the RSG wind depends on its velocity as $\rho(r) = \dot{M}_{\text{rsg}} / (4\pi r^2 v_{\text{rsg}})$, a low RSG wind velocity implies a much higher density. The expansion of the WR shell is faster for lower RSG wind densities and also for higher wind velocities. The termination shock of the WR wind is located at a much smaller radius than that of the hot MS bubble described in the previous section, so we simply assume free outflow as the outer boundary condition in order to calculate its dynamical behaviour (García-Segura et al. 1996a).

During the early stages, the swept-up WR shell is dense enough to be fully radiative. This ceases to be true, however, after the shell has extended to a radius of more than 0.1 pc, since its density decreases so much that its evolution becomes almost adiabatic. Correspondingly, the shell is initially thin and therefore subject to Vishniac instabilities (Vishniac 1983); but the increase of shell thickness soon suppresses the growth of the instability. This instability operates in dense winds where the cooling is effective enough to produce radiative terminal shocks. The RSG wind shell is accelerated by the (less dense) shocked WR wind and is therefore also subject to Rayleigh-Taylor (RT) and Vishniac instabilities. In this case we have a radiatively-cooled, thin, accelerated shell and the two instabilities must be coupled. The resulting structure after 8,000 yr of evolution since the onset of the WR phase is summarized in Fig. 3.

It is also possible for a fast WR wind to collide with early ejecta before it is decelerated by the RSG shell (or an Luminous Blue Variable (LBV) shell depending on the evolutionary pathway of the massive progenitor). To illustrate this, we study the last (unsteady) WR stage of a $60 M_{\odot}$ star. Mass loss lowers the stellar mass from $60 M_{\odot}$ all the way down to $\sim 4 M_{\odot}$ at the time of the final supernova (or GRB). The total mass loss includes $\sim 32 M_{\odot}$ lost in the MS and pre-LBV stages, $\sim 8 M_{\odot}$ lost in the LBV stage, and $\sim 16 M_{\odot}$ in the WR stage. The MS and LBV-WR stages have been modeled in a self-consistent fashion by García-Segura et al. (1996b). These stages have important implications for the circumstellar gas at $r \gg 0.4 \text{ pc}$. Here, we study the interaction between the fast-moving WR wind ($v_{\text{wr}} \sim 4000 \text{ km s}^{-1}$) just before the final supernova and the early, slower moving ($v_{\text{wr}} \sim 1500 \text{ km s}^{-1}$), ejecta⁷.

The resultant shell will be pushed outward by the central star wind and retarded by the early ejected wind, quickly reaching a constant velocity, but increasing in mass. The resulting expansion law for the shell follows from the momentum balance between the two components. The analytical theory of Kwok et al. (1978) can give some insight into the problem. If M_{ij} is the mass of the resulting shell when it is at a radial distance $r_{ij}(t)$, then

$$M_{ij}(t) = \int_{r_j+v_j t}^{r_{ij}(t)} \frac{\dot{M}_j}{v_j} dr + \int_{r_{ij}(t)}^{r_i+v_i t} \frac{\dot{M}_i}{v_i} dr, \quad (13)$$

where $v_j < v_i$. If $v_{ij}(t)$ is the velocity of the shell, then, assuming a completely inelastic collision, the equation of motion may be written

$$M_{ij}(t) \frac{d v_{ij}}{dt} = \frac{\dot{M}_i}{v_i} [v_i - v_{ij}]^2 - \frac{\dot{M}_j}{v_j} [v_j - v_{ij}]^2. \quad (14)$$

Numerical integration of equation (14), with a substitution for $M_{ij}(t)$ from equation (13) gives the resulting expansion law for the shell. The thickness of the shell Δr_{ij} may be found by requiring its internal pressure to balance the pressure from the wind.

Such large expansion velocities Δv_w produce high temperatures (see equation 7) in the post-shock region behind the outer shock of the merged shell. This high post-shock temperature and the low density (i.e. low \dot{M}_{wr} and high v_{wr}) of the WR wind result in an almost adiabatic, hot, low-density WR shell.

⁷ The reader is refer to Fig. 2 of García-Segura et al. (1996b) for the stellar mass-loss rates and wind velocities as a function of time for the $60 M_{\odot}$ model.

Figure 4 shows the morphology of the smooth WR ring under the assumption that the central star experiences non-spherical mass loss close to critical rotation: in other words, a scenario in which a slower and denser wind is confined to the equatorial plane. To compute the latitudinal dependence of the wind properties of a star close to critical rotation ideally requires multi-dimensional models of the star and its outflowing atmosphere, which are not available. Langer (1998), however, argued that the stellar flux and the radius might still vary only weakly from pole to the equator in very luminous stars. We therefore applied equations similar to those found by Bjorkman & Cassinelli (1993) for winds of rotating stars in the limit of large distance from the star:

$$v_\infty(\theta) = \zeta v_{\text{esc}} (1 - \Omega \sin \theta)^\varphi, \quad (15)$$

where we set the parameters defined in (Bjorkman & Cassinelli 1993) to $\zeta = 1$, $\varphi = 0.35$, $\Omega = v_{\text{rot}}/v_{\text{crit}}$, and $v_{\text{crit}} = v_{\text{esc}}/\sqrt{2} = [GM_*(1 - \kappa)R_*]^{1/2}$, with M_* and R_* being mass and radius of the star, and κ standing for the ratio L/L_{Edd} of stellar to Eddington luminosity (Langer et al. 1998). Under the above conditions, the wind expands more quickly and easily into the lower density wind at the poles, while stellar rotation concentrates it toward the equatorial plane, producing a double-lobed structure. In the following section we aim to examine the interaction of the relativistic blast wave with these more *realistic* density wind profiles.

5. THE AFTERGLOW APPEARANCE

The interaction of a relativistic blast wave with the surrounding medium is described by the adiabatic Blandford & McKee (1976; hereafter BM) self-similar solution. The scaling laws that are appropriate for the burst interaction with a medium with particle density $n \propto r^{-s}$ have been described by Mészáros et al. (1998), Chevalier & Li 2000, Panitescu & Kumar (2000), Ramirez-Ruiz et al. (2001), and Dai & Lu (2002).

For an adiabatic ultra-relativistic blast wave, the (isotropic equivalent) total energy is

$$E = \frac{8\pi A \Gamma^2 r^{3-s} c^2}{17-4s}, \quad (16)$$

where Γ is the bulk Lorentz factor of the shock front and r is the observed radius near the line of sight (BM). We assume the burst to be collimated with an initial half-angle θ larger than 20° , and that lateral expansion is negligible during the relativistic phase. A distant observer receives a photon emitted along the line of sight towards the fireball center at a time (Chevalier & Li 2000)

$$t = \frac{r}{4(4-s)\Gamma^2 c}, \quad (17)$$

and so

$$r = \left[\frac{(4-s)(17-4s)Et}{2\pi A c} \right]^{\frac{1}{(4-s)}}. \quad (18)$$

Before the collision with the high-density shell, the shock front is expected to propagate through an $n(r) = Ar^{-2}$ wind, where

$$A = 3 \times 10^{35} \dot{M}_{\text{wr},-5} v_{\text{wr},3}^{-1} \text{ cm}^{-1} \quad (19)$$

for a spherically symmetric wind ejected at a constant speed. The relativistic expansion is gradually slowed down until the shock front encounters the wind density discontinuity at a radius r_{sh} . A transition in the afterglow is then observed

$$t_{\text{sh}} \approx E_{52}^{-1} r_{\text{sh},17}^2 A_{35}^{-1} \text{ days} \quad (20)$$

after the burst. This of course only true for $r_{\text{sh}} < r_{\text{NR}}$ (see equation 4). This encounter produces two new shock waves: a forward shock that moves into the wind thin shell discontinuity and a reverse shock that propagates into the relativistic ejecta. In the section that follows we examine the state of these shocks under various assumptions regarding the density discontinuity.

5.1. Shock Conditions

Consider a relativistic shell with a Lorentz factor η moving into the cold circumburst medium (CM). The interaction is described by two shocks: a forward shock propagating into the CM and a reverse shock propagating into the ejecta. There are four regions separated by the two shocks: the CM (1), the shocked CM (2), the shocked ejecta (3) and the unshocked ejecta (4). The CM is at rest relative to the observer (Fig. 5). Velocities β_i , and their corresponding Lorentz factors γ_i , distances and time are measured relative to this frame. Thermodynamic quantities n_i , p_i and e_i (particle number density, pressure, and internal energy density) are measured in the fluids' rest frames. The ISM and the unshocked shell are cold and, therefore, $e_1 = e_2 = 0$. The shocked material is extremely hot and, therefore, $p_2 = e_2/3$ and $p_3 = e_3/3$ (Sari & Piran 1995).

For $\eta \equiv \gamma_4 \gg 1$ the equations governing the shocks are (3)

$$\frac{e_2}{n_2 m_p c^2} = \gamma_2 - 1 \approx \gamma_2; \quad \frac{n_2}{n_1} = 4\gamma_2 + 3 \approx 4\gamma_2 \quad (21)$$

$$\frac{e_3}{n_3 m_p c^2} = \bar{\gamma}_3 - 1; \quad \frac{n_3}{n_4} = 4\bar{\gamma}_3 + 3. \quad (22)$$

The approximations in equation (21) use only the fact that $\gamma_4 \gg 1$ and therefore $\gamma_2 \gg 1$. No assumption is made about $\bar{\gamma}_3$, the Lorentz factor of the motion of the shocked material in region (3) relative to the unshocked shell in region (4).

Equality of pressures and velocities along the contact discontinuity yields

$$e_2 e_3; \quad \bar{\gamma}_3 \approx \frac{1}{2} \left(\frac{\gamma_4}{\gamma_2} + \frac{\gamma_2}{\gamma_4} \right). \quad (23)$$

The solution for γ_2 depends only on two parameters, η and $\psi \equiv n_4/n_1$. The energy, pressure, and density also depend linearly on a third parameter, the external density n_1 (Sari & Piran 1995).

There are two simple limits of equations (21)-(23) in which the reverse shock is either Newtonian or ultra relativistic (the forward shock is always ultra relativistic if $\eta \gg 1$ and $\psi > \eta^{-2}$). If $\eta^2 \gg \psi$, the reverse shock is ultra relativistic ($\bar{\gamma}_3 \gg 1$):

$$\bar{\gamma}_3 = \frac{\sqrt{\eta}}{\sqrt{2}\psi^{1/4}}; \quad \gamma_2 = \gamma_3 = \frac{\sqrt{\eta}\psi^{1/4}}{\sqrt{2}}. \quad (24)$$

In this case almost all of the initial kinetic energy is converted by the shocks into internal energy ($\eta \gg \gamma_3$). The process therefore is over after a single passage of the reverse shock through the ejecta (Sari & Piran 1995).

If $\psi \gg \eta^2$ the reverse shock is Newtonian ($\bar{\gamma}_3 - 1 \ll 1$) and

$$\bar{\gamma}_3 \approx \frac{4\eta^2\psi^{-1}}{7} \equiv 2\epsilon \ll 1; \quad \gamma_2 = \gamma_3 = \eta(1 - \sqrt{\epsilon}). \quad (25)$$

The reverse shock converts only a fraction $\gamma/\sqrt{\psi} \ll 1$ of the kinetic energy into internal energy. It is too weak to slow down the ejecta effectively, and most of the initial energy is still kinetic energy when this shock reaches the inner edge of the ejecta.

In any realistic situation the CM is probably inhomogeneous, as in the stellar models described in the previous section. Consider a density jump by a factor α over a distance λ . The forward shock propagates into the CM with a density n_1 as before, and when it reaches the position where the CM density is αn_1 a new shock wave is reflected. This shock is reflected again off the shell. The reflection time is about $\lambda/(4c\alpha^{1/2})$. After these reflections, the Lorentz factor and hydrodynamical properties of the system are as if the CM were homogeneous with a density αn_1 .

For an adiabatic blast wave, the corresponding observer peak frequency is $\nu_m \propto B\gamma_e^2/(m_e c)$, where $B \approx \sqrt{32\pi c\epsilon_B^{1/2} m_p^{1/2} n_1^{1/2} \eta}$ is the turbulently generated magnetic field (assumed to be amplified up to a fraction ϵ_B by the processes in the shocked region and not determined directly by the field in the WR star). The emission at low frequencies ($\nu \ll \nu_m$) scales as $\nu^{1/3}$ and at high frequencies ($\nu \gg \nu_m$) it scales as $\nu^{-(p-1)/2}$. The ratio of $\nu_{m,\alpha}$, the observed peak frequency from the relativistic shell after the forward shock has traversed a density jump of a factor α over a distance λ , and the frequency in the absence of such a jump ν_m is

$$\frac{\nu_{m,\alpha}}{\nu_m} \approx \frac{\eta_\alpha^4 (\alpha n_1)^{1/2}}{\eta^4 n_1^{1/2}} \approx \alpha^{-1/2}. \quad (26)$$

Therefore, we expect this emission to be a significant contribution to the long-wavelength flux. At late times, when the collision has run its course, the shells have merged back to a Blandford & McKee solution and the observed flux is proportional to $E_\alpha^{(p+1)/[2(4-s)]}$. In the absence of a density enhancement, the flux would have been proportional to $E^{(p+1)/[2(4-s)]}$. Therefore, the increase in the observed emission from the forward shock due to the density jump is approximately $(E_\alpha/E)^{(p+1)/[2(4-s)]} \approx \alpha^{(p+1)/[4(4-s)]}$, neglecting the enhanced energy losses from the shocks that may arise during the collision with the high-density thin shell. We should expect, however, a smooth transition from one solution to the other at most wavelengths. This is not the case at frequencies for which there is significant emission from the reverse shock, from which the total emission is smaller and at a lower frequency by typically a factor of η . At these frequencies the impact of this additional emission is likely to be significant.

5.2. Afterglow Lightcurves

We now generalize the above results to a spatially varying external density. The afterglow modeling used here is similar to that described in Salmonson (2003). The jet deceleration is calculated from the mass and energy conservation equations. The lateral spreading of the jet is neglected. The calculation of radiative losses includes synchrotron emission, and the synchrotron spectrum is taken to be a piecewise power law with the usual self-absorption, cooling, and injection break frequencies, calculated from the cooled electron distribution and magnetic field. The observed flux is obtained by integrating the jet emission over the equal arrival time surface.

Strong temporal variations compared to the canonical power-law decay can be produced by changes in the circumburst density or by energy variations (e.g. Meszaros et al. 1998). For example, as shown in Ramirez-Ruiz, Merloni & Rees (2001), a shock wave that has been slowed by the surrounding medium could be caught up by subsequent shocks, increasing the shock wave energy. Alternatively, the shock wave's energy may have varied as the result of encountering an external medium of variable density. While here we concentrate on the case where the dominant variations are in density, the two alternatives can be distinguished by exploiting the fact that the flux at $\nu_c < \nu$ is insensitive to variations in the ambient density, whereas below the cooling frequency $F_\nu(\nu_c < \nu) \propto n^{1/2}$ (Nakar et al. 2003; Heyl & Perna 2003). As the blast wave expands into the ambient matter, its kinetic energy is used to shock and heat the matter. Deceleration due to this starts in earnest when about half the initial energy is transferred to the shocked matter. The characteristic mass M_{dec} where this takes place is given by equation (3). This phase ends when so much mass shares the energy that the Lorentz factor drops to 1. This occurs at a mass scale M_{NR} (see equation 4).

In the case depicted in Fig. 3, for example, the stellar wind is not dense enough to slow down the ejecta to non-relativistic speeds before reaching r_{sh} , so that we expect part of the blast wave evolution as we see it to take place outside the $1/r^2$ density distribution. In a rarefied wind such as that illustrated in Fig. 4, the shock front will expand within the stellar wind until it reaches the density discontinuity at about 0.2 pc without significant deceleration. Over the typical time of observation of a GRB afterglow, the impact of the relativistic ejecta with the density enhancement will produce a clear feature in the observed emission. Fig. 6 and its caption summarize the predicted R-band afterglow lightcurve from hours until about a few years after the burst. One can see sharp break in the flux decay curve that coincides with a precipitous drop in Lorentz factor when the afterglow shock meets the shell. In this model, the isotropic energy of the ejecta is 5×10^{53} erg. The characteristic synchrotron frequency is lower than that in the absence

of the collision. This effect is responsible for the decrease in flux (at a fixed frequency) seen at about ~ 10 days. Further observable transitions are produced as the blast-wave plows deeper into the shocked-wind discontinuity. Jet effects are expected to become important at a time

$$t_j \approx 5(\theta_j/0.08)^4 (E/10^{53} \text{ erg})(A/10^{35} \text{ cm}^{-1})^{-1} \text{ days}, \quad (27)$$

just before the impact takes place. This makes the jet-break time not easily identifiable.

The evolution of the apparent source size is shown in Fig. 7. The afterglow image is limited to a circle on the sky, whose size grows as $t^{(5-s)/2(4-s)}$ (Granot & Loeb 2001). The assumption of a spherical flow may also serve as an adequate description of a jetted flow, at sufficiently early times before the jet break time, t_j , when the Lorentz factor of the flow drops below the inverse of the jet opening angle (Rhoads 1997). In the case of a jet, the image at $t \gtrsim t_j$ is expected to be different than in the spherical case (Oren, Nakar & Piran 2004; Granot, Ramirez-Ruiz & Loeb 2004) and will no longer be circular for observers who are situated away from the jet axis (Fig. 7). The image size depends decisively on the density profile of the ambient medium into which the GRB fireball propagates. The effects of the density discontinuity on the size of the afterglow image can be seen by comparing the solid and dashed curves in Fig. 7. This is not altogether surprising: the ejected material is decelerated by the external medium at a smaller radius than it would be in the absence of the density discontinuity. The calculations above demonstrate how the measurable properties of such afterglows depend on the nature of the progenitor star and the medium around it.

6. CLUMP FORMATION AND AFTERGLOW VARIABILITY

The smoothness or clumpiness of the swept-up shell may be responsible for small-scale variability observed in many gamma-ray burst afterglows. As illustrated in Fig. 4, the required degree of clumping in the Wolf-Rayet star wind itself does not seem plausible. On the other hand, as shown in Fig. 3, there is the possibility of clump development from the swept up RSG wind. As stated above, the shocked RSG wind is accelerated by the (less dense) shocked WR wind and is therefore subject to RT instabilities. The shell is initially thin and is therefore also subject to Vishniac instabilities. The two instabilities must then be coupled. The coupling mechanism appears to be a displacement of gas towards the interior of the bubble at the contact surface by the RT instability, which induces the formation of a valley in the outer shock, driving what is fundamentally a Vishniac instability. García-Segura et al. (1996b) found that clump formation is not efficient for the case of pure RT instabilities in thick shells and concluded that a necessary condition for clump formation to occur is that a shell be thin enough to allow Vishniac-like instabilities to drive transverse motions to form the clumps. Many RT fingers will then warp and break, forming knots.

Once formed, the knots tend to dissipate. Several processes tend to destroy the inhomogeneities embedded in a wind-blown bubble, namely thermal evaporation (Cowie & McKee 1977), ablation (Hartquist et al. 1986) and photo-evaporation (McKee 1986). If not inhibited by the presence of a magnetic field, heat conduction may deplete the clumps. The thermal evaporation time is

$$t_{\text{ev}} \propto \frac{n_c T_{\text{sw}} \Delta r}{n_{\text{sw}}}, \quad (28)$$

where T_{sw} is the temperature of the hot shocked WR wind, Δr and n_c are, respectively, the radii and densities of the clumps, and n_{sw} is the shocked wind density. For $n_c \geq 10n_{\text{sw}}$, $T_{\text{sw}} \sim 4 \times 10^7 \text{ K}$ and $\delta r \leq 0.01 \text{ pc}$ one has $t_{\text{ev}} \leq 10^4$, so that, if conduction is unimpeded, the lifetime of the clumps may be shorter than the nebula lifetime. Erosion via ablation is far less effective, and the clumps survive if, as expected (see e.g. Hartquist et al. 1986), heat conduction is inefficient. The ablation time for a knot is

$$t_{\text{ab}} \propto \frac{n_c \Delta r}{n_{\text{sw}} v_{\text{rsg}}}. \quad (29)$$

We estimate $t_{\text{ab}} \geq 10^2 t_{\text{ev}}$. The characteristic photo evaporation time of a clump at a distance r from a star emitting S ionizing photons per second is

$$t_{\text{pe}}(r) \propto n_c \frac{\Delta r^{3/2}}{S^{1/2}} r. \quad (30)$$

For the clump parameters considered above and $S = 10^{49} \text{ s}^{-1}$ one has $t_{\text{pe}} \sim 10^4 r_{\text{pc}} \text{ yr}$. Small neutral condensations are thus likely to be photo-evaporated while larger ones survive.

The jet will then encounter clumps – if they are not efficiently destroyed – with large variations in density. Presumably the clump is symmetric such that

$$\Delta r_{\parallel} = \Delta r_{\perp} = \Delta r_{\text{clump}}. \quad (31)$$

Whether or not the ambient object collapses onto the shell is a key distinction that must be made in order to understand how the clump determines the time structure. We assume here the case of a "collapsible" object (such as a wind clump). The contribution to the peak duration from the time the jet takes to move through the clump $r_{\text{clump}}/(\gamma^2 c)$, is negligible compared with the time the shell takes to engage the perpendicular size of the object. This engagement time is caused by the curvature of the jet. The curvature of the expanding jet prevents it from engaging the cloud instantaneously. Rather, the portion of the jet at $\theta \sim \gamma^{-1}$ requires a time $r(1 - \cos\theta)/v$ longer to reach the cloud. At an angle θ from the line of sight, the time to engage the object is $\theta r_{\text{clump}}/2c$. At a typical angle of $\theta \sim \gamma^{-1}$,

$$\Delta t = \frac{2r_{\text{clump}}}{c\gamma}. \quad (32)$$

The alternative is that the ambient source does not collapse, but produces photons on a scale of Δr_{clump} (unlikely). The timescale in this case is determined from the light travel time across the overlap of the shell thickness and the ambient source thickness. If

the clumps where distributed as a power-law of clump sizes, one might expect a power law distribution of observable peak widths. The cumulative effect of many small-scale density perturbations will tend to average out during the expansion history of the jet, and, therefore, the resultant afterglow profile should be relatively smooth. An upper limit on Δr_{clump} is set by observed afterglow variability timescales (i.e. Δt_{obs}), where

$$c\Delta t_{\text{obs}} < \Delta r_{\text{clump}} < \frac{c\Delta t_{\text{obs}}\gamma}{2}. \quad (33)$$

Short time scale of afterglow oscillations provide interesting upper limits of $\Delta r_{\text{amb}} \leq 10(\gamma/10)$ AU on the size of the clumps around GRB 011211 (Jakobsson et al. 2004) and GRB 030329 (Lipkin et al. 2004). These limits are lower than the fluctuation amplitudes seen on similar scales in the local interstellar medium (Wang & Loeb 1999), though they may reflect the length scale of comet-like clumps produced in ring nebulae surrounding massive stars.

7. DISCUSSION

It is evident from the above discussion that the environment of a massive star at the time of its death is a very rich one. Even in the simplest case of a wind whose properties do not vary over the life of the star, complex behaviour with multiple possible transitions in the observable part of the afterglow lifetime may be seen. The eventual resulting afterglow lightcurve depends fairly strongly on the properties of the system, especially the mass-loss rate of the star and the ambient density. This has a good and a bad side. On the negative side, it implies that one can not be too specific about the times at which we expect to see transitions in the observed emission. On the positive side, if and when we do see these transitions, they can be fairly constraining on the properties of the stellar progenitor.

Considering the radial range relevant to GRBs, the absence of the expected $1/r^2$ density structure in many bursts is not surprising. On the other hand, the reason for low densities remains unclear. A wind termination shock may resolve this matter although very special conditions are necessary to bring this about. Because the density in a shocked wind is higher than that in a free wind at the same radial distance, the low-density requirement is not alleviated by appealing to a shocked WR wind. A low stellar mass wind loss, a faster wind velocity or a low metallicity may help, although it is not clear whether realistic assumptions can provide the required low densities (Wijers 2001; Chevalier et al. 2004). The following point should be emphasized here. The fireball model used to infer the circumburst density is highly simplified. For example, the wind density is assumed to follow a pure $1/r^2$ law and to be free of inhomogeneities, the expanding jet surface is assumed uniform with no internal (density, velocity) gradients and the fraction of the explosion energy in the post shock magnetic field is assumed to be constant (Panaitescu & Kumar 2002). We do not know whether a description of the afterglow data is possible with a wide variety of underlying assumptions and whether that would substantially change the parameters inferred. Still, the low densities inferred by afterglow observations are thus problematic for the collapsar model.

The task of finding useful progenitor diagnostics is simplified if the pre-burst evolution leads to a significantly enhanced gas density in the immediate neighborhood of the burst. The detection of spectral signatures associated with the GRB environment would provide important clues about the triggering mechanism and the progenitor. A special case is that of GRB 021004, where lines of highly ionized species, blueshifted relative to the host galaxy, have been attributed to a Wolf-Rayet stellar wind (Mirabal et al. 2003; Schaefer et al. 2003). Stars interact with the surrounding interstellar medium, both through their ionizing radiation and through mass, momentum and energy transfer in their winds. Mass loss leads to recycling of matter into the interstellar medium, often with chemical enrichment. Mass loss is a significant effect in the evolution of massive stars; in particular, for stars that enter WR stages (e.g. Ramirez-Ruiz et al. 2001). WR stars follow all or part of the sequence WNL, WNE, WC and WO, which corresponds to a progression in the exposure of nuclear products (CNO equilibrium with H present, CNO equilibrium without H, early visibility of the products of the 3α reaction and then a growing (C+O)/He ratio respectively). Mass loss drastically influences stellar yields. At low Z there is a high production of α -nuclei, while at higher Z most of the He and C produced is ejected in stellar winds and escapes further nuclear processing. This characteristic offers a direct observational test of which stars are likely to produce a GRB.

Finally, The total energy observed in γ -rays from GRBs whose redshift has been determined is diverse (e.g. Soderberg et al. 2004). One appealing aspect of a massive star progenitor is that the great variety of stellar parameters can probably explain this diversity. Given the need for a large helium core mass in progenitors, the burst formation may be favored not only by rapid rotation but also by low metallicity. Larger mass helium cores might have more energetic jets, but it is unclear whether they can be expected to be accelerated to large Lorentz factors (MacFadyen, Woosley & Heger 2001; Ramirez-Ruiz, Celotti & Rees 2002). Many massive stars may produce supernovae by forming neutron stars in spherically symmetric explosions, but some may fail neutrino energy deposition, forming a black hole in the center of the star and possibly a GRB. One expects various outcomes ranging from GRBs with large energies and durations, to asymmetric, energetic supernovae with weak GRBs (Totani 2003; Granot & Ramirez-Ruiz 2004). The medium surrounding a GRB would provide a natural test to distinguish between different stellar explosions.

We thank M. J. Rees, J. Granot, R. Chevalier, S. Woosley and N. Langer for helpful discussions. This work is supported by NASA through a Chandra Postdoctoral Fellowship award PF3-40028 (ER-R). GG-S acknowledged support from CONACYT 43121 grant.

REFERENCES

- | | |
|---|--|
| Bloom, J. S., et al. 1999, <i>Nature</i> , 401, 453 | Chevalier, R. A., & Li, Z. 2000, <i>ApJ</i> , 536, 195 |
| Bjorkman, J. E., & Cassinelli, J. P. 1993, <i>ApJ</i> , 409, 429 | Chevalier, R. A., Li, Z., & Fransson, C. 2004, <i>ApJ</i> , 606, 369 |
| Blandford, R. D., & McKee, C. F. 1976, <i>Phys. Fluids</i> , 19, 1130 | Chiosi, C., & Maeder, A. 1986, <i>ARA&A</i> , 24, 329 |
| Blondin, J. M., & Lundquist, P. 1993, <i>ApJ</i> , 405, 337 | Clarke, D. A. 1996, <i>ApJ</i> , 457, 291 |
| Castor, J., McCray, R., & Weaver, R. 1975, <i>ApJ</i> , 200, L107 | Cowie, L. L., & McKee, C. F. 1977, <i>ApJ</i> , 211, 135 |
| Chevalier, R. A., & Liang, E. P. 1989, <i>ApJ</i> , 344, 332 | Dai, Z., & Lu, T. 2002, <i>ApJ</i> , 565, L87 |

- Djorgovski, S. G., et al. 2001, *ApJ*, 562, 654
- Franco, J., et al. 1991, *PASP*, 103, 803
- Fransson, C., Lundquist, P., Chevalier, R. A. 1996, *ApJ*, 461, 993
- Fruchter, A. S., et al. 1999, *ApJ*, 519, L13
- Galama, T., et al., 1998, *Nature*, 387, 479
- García-Segura, G., Langer, N., & Mac Low, M. M. 1996a, *A&A*, 316, 133
- García-Segura, G., Mac Low, M. M., & Langer, N. 1996b, *A&A*, 305, 229
- García-Segura, G., & Franco, J. 1996, *ApJ*, 469, 171
- García-Segura, G., & Mac Low M.-M. 1995a, *ApJ*, 455, 145
- García-Segura, G., & Mac Low M.-M. 1995b, *ApJ*, 455, 160
- Granot, J., & Loeb, A. 2001, *ApJ*, 551, L63
- Granot, J., & Ramirez-Ruiz, E. 2004, *ApJ*, 609, L9
- Granot, J., Ramirez-Ruiz, E., & Loeb, A. 2004, *ApJ* in press (astro-ph/0407182)
- Hartquist, T. W., et al. 1986, *MNRAS*, 221, 715
- Heyl, J. S., & Perna, R. 2003, *ApJ*, 586, L13
- Hjorth, J., et al., 2004, *Nature*, 423, 847
- Izzard, R. G., Ramirez-Ruiz, E., & Tout C. A., 2004, *MNRAS*, 348 1215
- Jakobsson, P., et al. 2004, *NewA*, 9, 435
- Königl, A., & Granot, J. 2002, *ApJ*, 574, 134
- Kwok, S., Purton, C. R., & Fitzgerald, P. M. 1978, *ApJ*, 219, L125
- Langer, N. 1998, *A&A* 329, 551
- Langer N., Kiriakidis M., El Eid M.F., Fricke K.J., Weiss A., 1988, *A&A*, 192, 177
- Langer, N. 1991, *A&A*, 252, 669
- Lipkin, Y. M., et al. 2004, *ApJ*, 606, 381
- MacFadyen, A. I., & Woosley, S. E., 1999, *ApJ*, 524, 262
- MacFadyen, A. I., Woosley, S. E., & Heger, A. 2001, *ApJ*, 550, 410
- McKee, C. F. 1986, *Ap&SS*, 118, 383
- Mészáros, P., Rees, M. J., & Wijers, R. 1998, *ApJ*, 499, 301
- Mirabal, N., et al. 2003, *ApJ*, 595, 935
- Nakar, E., Piran, T., & Granot, J. 2003, *NewA*, 8, 495
- Oren, Y., Nakar, E., & Piran, T. 2004, *MNRAS*, 353, L35
- Ostriker, J. P., & McKee, C. F. 1988, *Rev. Mod. Phys.*, 60, 1
- Paczynski, B. 1998, *ApJ*, 494, L45
- Panaitescu, A., & Kumar, P. 2000, *ApJ*, 543, 66
- Panaitescu, A., & Kumar, P. 2002, *ApJ*, 571, 779
- Piro, L., et al. 2000, *Science*, 290, 955
- Ramirez-Ruiz, E., Dray, L., Madau, P., & Tout, C. A. 2001, *MNRAS*, 327, 829
- Ramirez-Ruiz, E., Merloni, A., & Rees, M. J. 2001, *MNRAS*, 324, 1147
- Ramirez-Ruiz, E., Celotti, A., & Rees, M. J. 2002, *MNRAS*, 337, 1349
- Reeves, G. D., et al. 2002, *Nature*, 416, 512
- Rhoads, J. E. 1997, *ApJ*, 487, L1
- Salmonson, J. D. 2003, *ApJ*, 592, 1002
- Sari, R., & Piran, T. 1995, *ApJ*, 455, L143
- Schaefer, B. E., et al. 2003, *ApJ*, 588, 387
- Soderberg, A. M., Ramirez-Ruiz, E. 2003, *MNRAS*, 345, 854
- Soderberg, A. M., et al. 2004, *Nature*, 430, 648
- Stanek, K. Z., et al., 2003, *ApJ*, 591, L17
- Stone, J. M., & Norman, M. L. 1992, *ApJS*, 80, 753
- Totani, T. 2003, *ApJ*, 598, 1151
- Trentham, N., Ramirez-Ruiz, E., & Blain, A. W. 2002, *MNRAS*, 334, 983
- Vietri, M., & Stella, L. 1998, *ApJ*, 507, L45
- Vishniac, E. T. 1983, *ApJ*, 274, 152
- Wang, X., & Loeb, A. 2000, *ApJ* 535, 788
- Waxman, E., Frail, D., & Kulkarni, S. 1998, *ApJ*, 497, 288
- Weaver, R., et al. 1977, *ApJ*, 218, 377
- Wijers R. A. M. J., et al. 1998, *MNRAS*, 294, L13
- Wijers, R. A. M. J. 2001, in *Gamma Ray Bursts in the Afterglow Era*, ed. E. Costa, Frontera F. and Hjorth J. (Springer: Berlin), 306
- Woltjer, L. 1972, *ARA&A*, 10, 129
- Woosley, S. E. 1993, *ApJ*, 405, 273
- Zeh, A., Klose, S., & Hartmann, D. H. 2004, *ApJ*, 609, 952
- Zhang, W., Woosley, S. E., & MacFadyen, A. I. 2003, *ApJ*, 586, 356

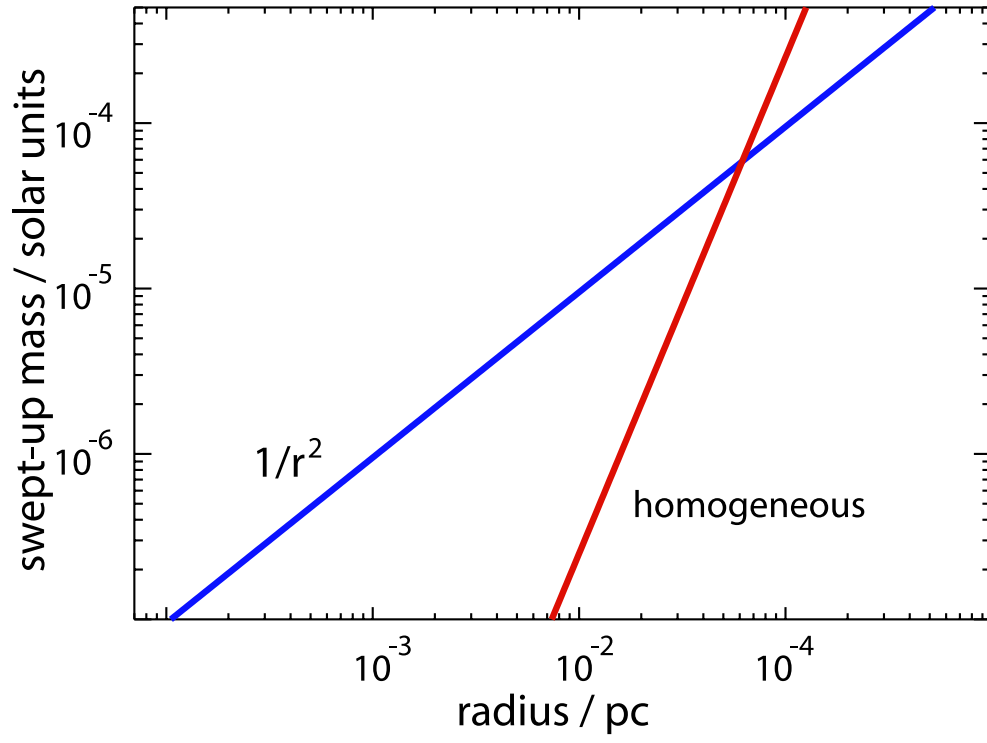


FIG. 1.— Constraints on the swept-up mass M as a function of radius. The blue line is the swept-up wind mass assuming $\dot{M} = 10^{-6} M_{\odot} \text{yr}^{-1}$ and $v_w \sim 10^3 \text{km s}^{-1}$. The red line, on the other hand, assumes a uniform medium with 1 cm^{-3} .

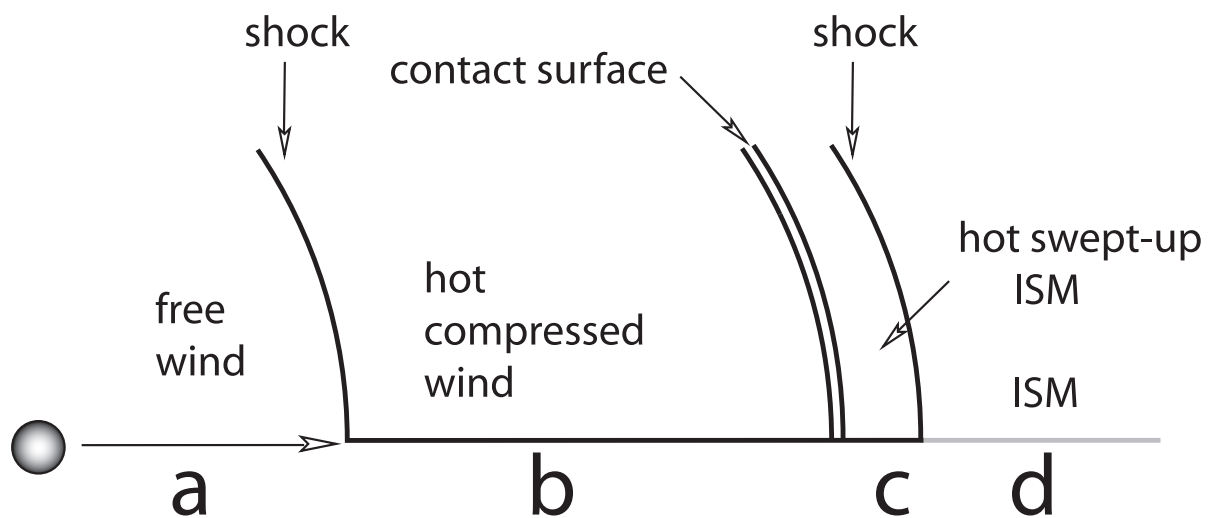


FIG. 2.— The formation of shocks by a stellar driven wind interacting with the surrounding interstellar medium. The interaction leads to a driven wave composed of shock compressed wind, a contact surface, and the swept-up ISM. Fast stellar wind matter (zone [a]) enters the shock where it is compressed by a factor of ~ 4 , and heated; the accumulated shock wind material is in zone (b). The entire region between the two shocks is nearly isobaric, so if material cools, it becomes compressed and resides in the contact surface, which forms a boundary between the shocked wind and the shocked, swept-up ISM (zone [c]). The undisturbed ISM is in zone (d).

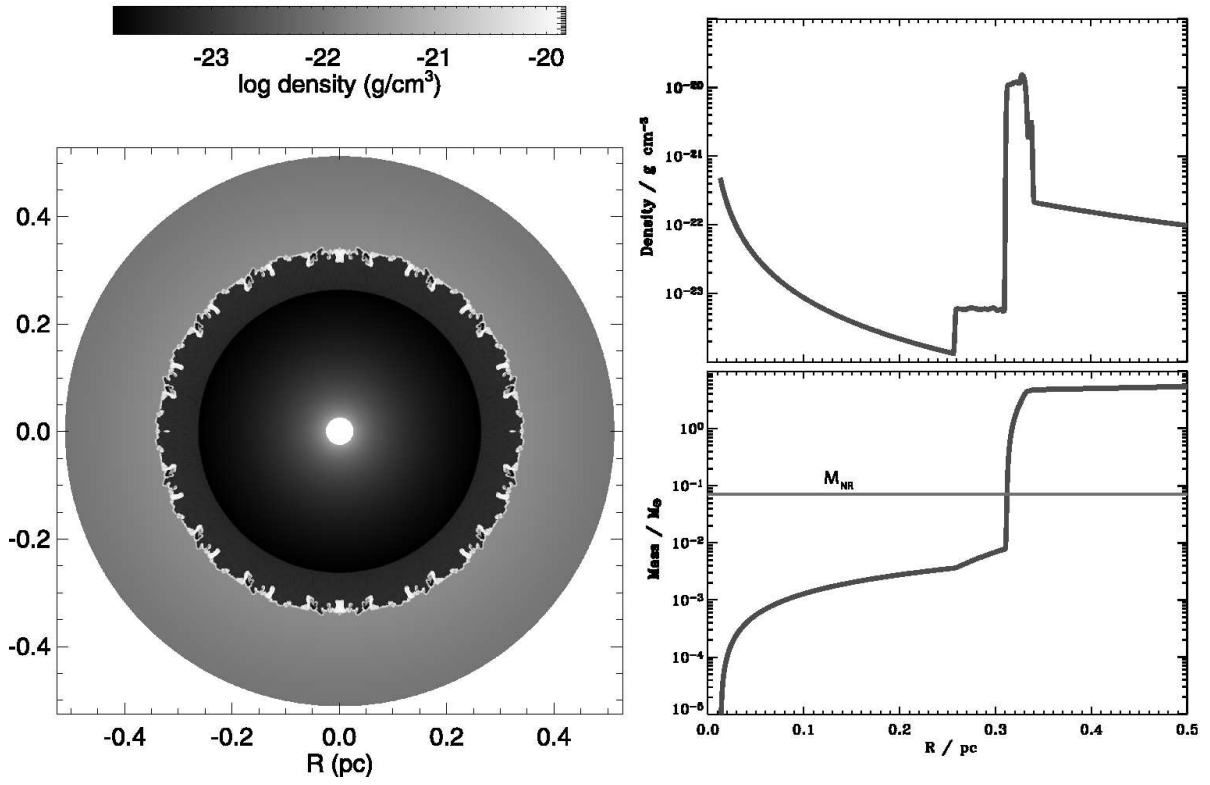


FIG. 3.— The state of the circumstellar medium around a $29 M_{\odot}$ massive star after 8,000 yr of evolution since the onset of the WR phase. The grid has 800×180 zones, with a radial extent of 0.5 pc and an angular extent of 22.5° . The inner-most radial zone lies at 0.0125 pc. *Left panel:* Logarithm of the circumstellar density in units of g cm^{-3} . *Right Panel:* Density and cumulative mass as a function of radius along the polar axis.

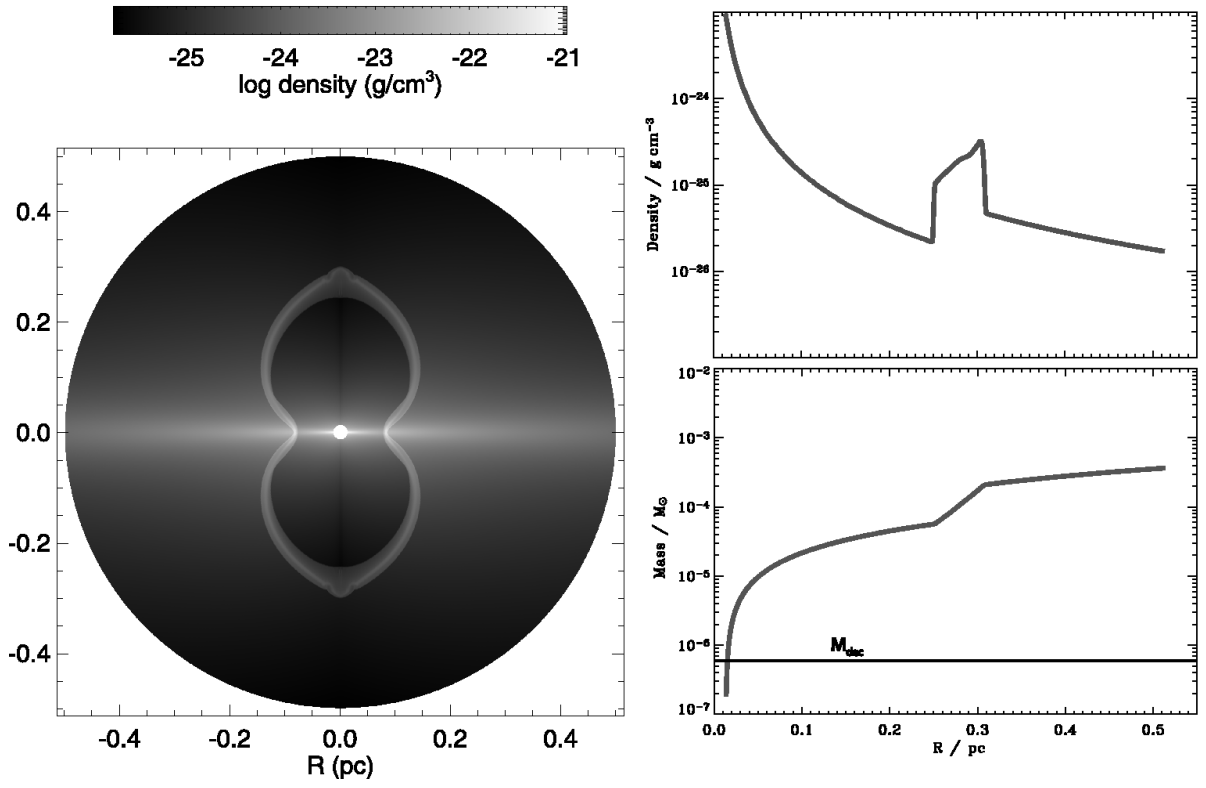


FIG. 4.— The state of the nearby circumstellar medium around a $60 M_{\odot}$ rotating massive star. During the last stages within its WR lifetime, the wind velocity increases. The fast wind collides with early ejecta before reaching the LBV shell. The grid has 800×180 zones, with a radial extent of 0.5 pc and an angular extent of 90° . The inner-most radial zone lies at 0.0125 pc. *Left panel:* Logarithm of the circumstellar density in units of g cm^{-3} . *Right Panel:* Density and cumulative mass as a function of radius along the polar axis.

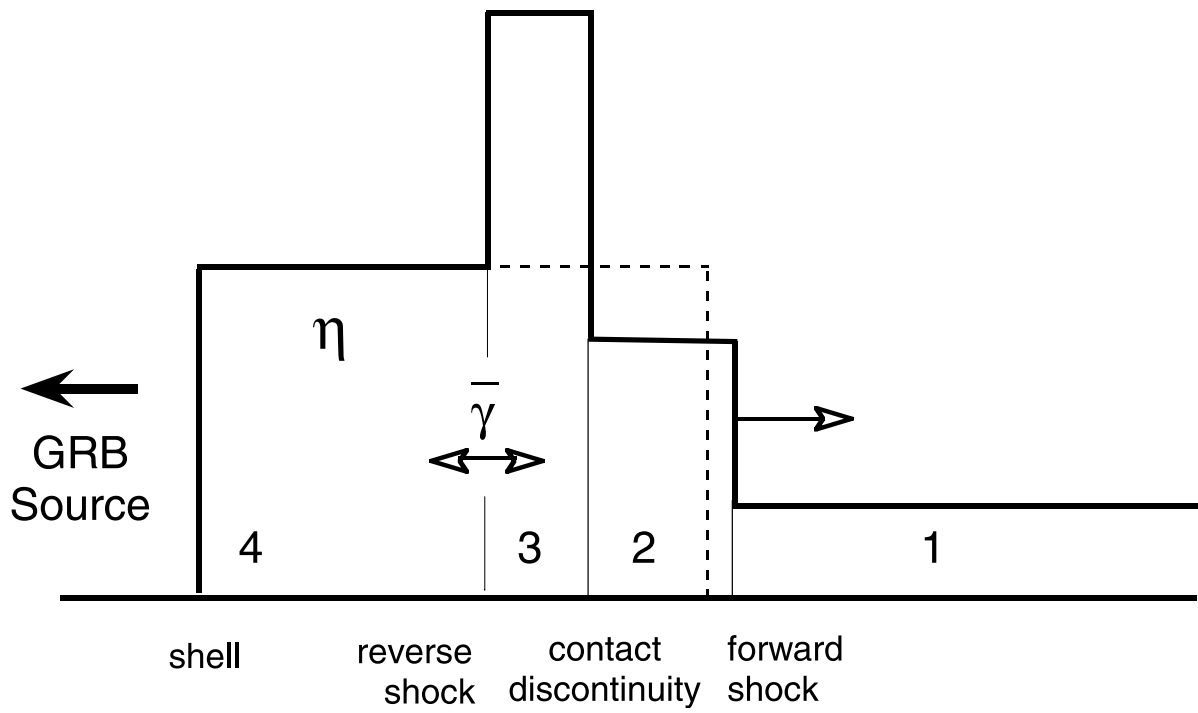


FIG. 5.— Diagram illustrating a relativistic shock system. Basic system consisting of a shocked fluid encountering matter at rest. Quantities for the system are the unshocked ejecta, the reverse and forward shocks, and the external matter at rest.

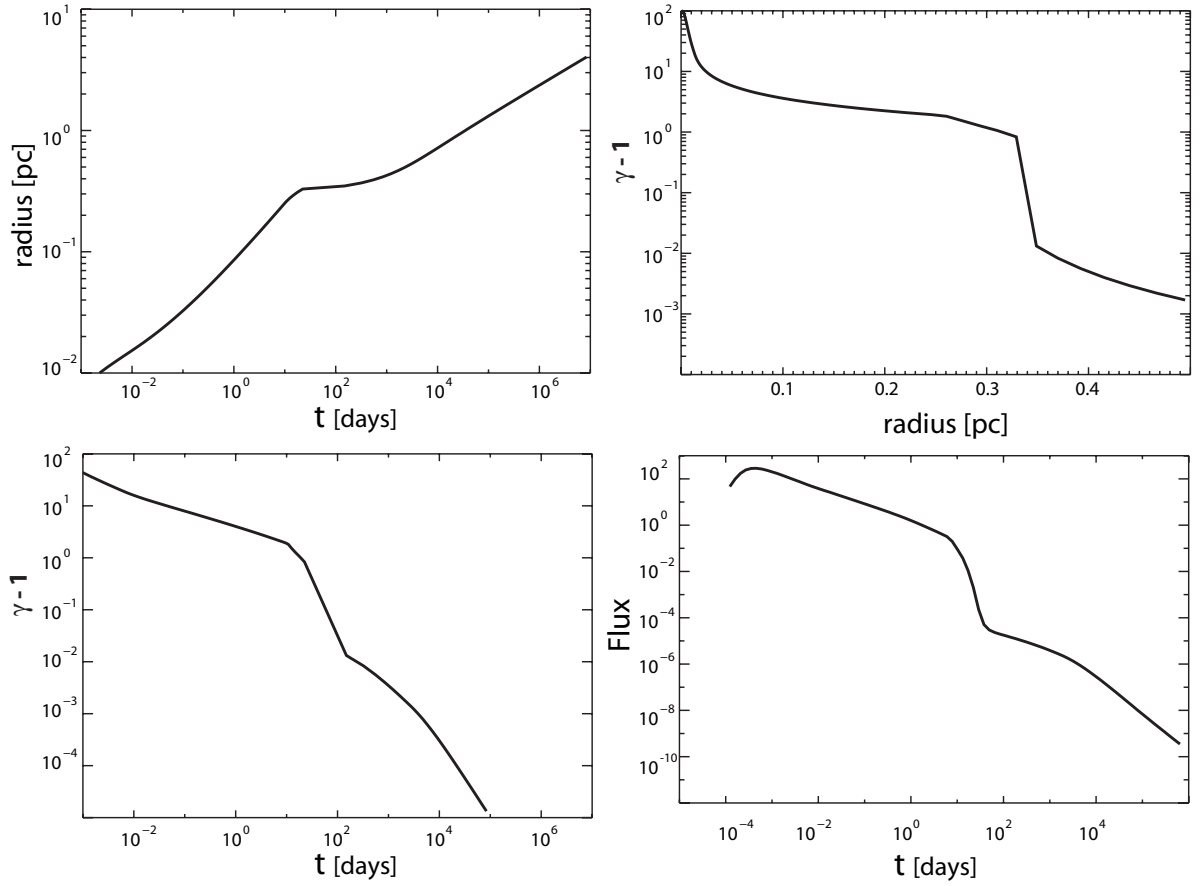


FIG. 6.— The effect of the impact of a relativistic jet with the wind density discontinuity on the R-band afterglow. The shock front expands within the $s = 2$ stellar wind until it reaches the high-density shell at a distance $r_{\text{sh}} \approx 0.2$ pc (see Fig. 3). The shock transit of the massive shell causes a rapid decline in Lorentz factor and a corresponding decline in flux. The remaining evolution of the shock is non-relativistic. At the time of the collision the relativistic shell Lorentz factor is $\gamma \sim 4$ for $E = 5 \times 10^{53}$ ergs. In this simulation the jet opening angle is $\theta_j = 5^\circ$ and it is viewed at $\theta_{\text{obs}} = 3^\circ$ from the jet axis. The afterglow emission is calculated in the adiabatic regime. The collision model takes into account the fireball geometrical curvature when calculating the photon arrival time and relativistic boosting.

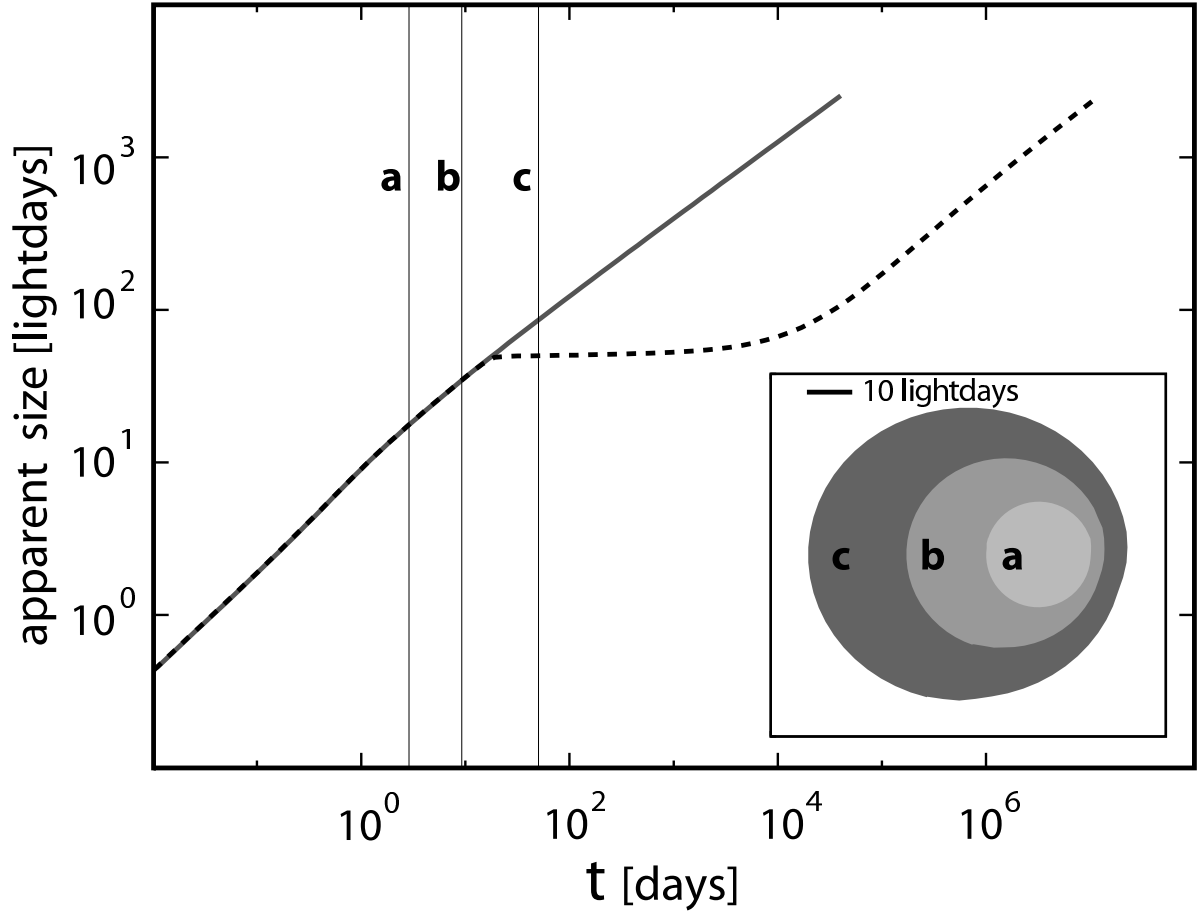


FIG. 7.— Evolution of the afterglow source size as a function of time for a sharp-edged, homogeneous jet seen at $\theta_{\text{obs}} = 0.6\theta_j = 3^\circ$. This one dimensional, hydrodynamic model takes on the density profile of the stellar wind in the polar direction. The jet deceleration is calculated from the mass and energy conservation equations. The lateral spreading of the jet is neglected. The effect of the impact of a relativistic jet with the wind density discontinuity (Fig. 3) can be seen by comparing the solid and dashed curves. The inset panel shows the afterglow source diameter. The x- and y-axes are shown in their true scale and measured in light-days.